

Einstein Probe Discovery of an X-ray Flare from K-type Star PM J23221-0301

Guoying Zhao (赵国英)^{a,b}, WeiKang Zheng^c, Rong-Feng Shen (申荣锋)^{a,b}, Qingcang Shui^d, Dongyue Li^e, Chang Zhou^f, Tianci Zheng^g, Weimin Yuan^e, Chong Ge^h, Junfeng Wang^h, Alexei V. Filippenko^c, Thomas G. Brink^c, Jordan Formanⁱ, Mayra Gutierrezⁱ, Isabelle Jonesⁱ, Ravjit Kaurⁱ, Naunet Leonhardes-Barbozaⁱ, Petra Mengistuⁱ, Avi Patelⁱ, Andrew Skemerⁱ, Anavi Uppalⁱ, Nicole Wolffⁱ, Michele N. Woodlandⁱ

^a*School of Physics and Astronomy, Sun Yat-Sen University, Zhuhai, 519000, Guangdong, China*

^b*CSST Science Center for the Guangdong-Hongkong-Macau Greater Bay Area, Sun Yat-Sen University, Zhuhai, 519082, China,*

^c*Department of Astronomy, University of California, Berkeley, CA 94720-3411, USA*

^d*Key Laboratory of Particle Astrophysics, Institute of High Energy Physics, Chinese Academy of Sciences, 100049, Beijing, China*

^e*National Astronomical Observatories, Chinese Academy of Sciences, 20A Datun Road, Chaoyang District, 100101, Beijing, China*

^f*Department of Astronomy, School of Physics, Huazhong University of Science and Technology, Wuhan, 430074, Hubei, China*

^g*Purple Mountain Observatory, Chinese Academy of Sciences, Nanjing, 210023, Jiangsu, China*

^h*Department of Astronomy, Xiamen University, Xiamen, 361005, Fujian, China*

ⁱ*Department of Astronomy & Astrophysics, University of California, Santa Cruz, CA 95064-1077, USA*

arXiv:2512.16679v1 [astro-ph.HE] 18 Dec 2025

Abstract

Stellar flares are an intense stellar activity that can significantly impact the atmospheric composition of the surrounding planets and even the possible existence of life. During such events, the radiative energy of the star is primarily concentrated in the optical and X-ray bands, with the X-ray flux potentially increasing by tens or even hundreds of times. Einstein Probe (EP) detected a new X-ray transient EP J2322.1-0301 on 27 September 2024. Its spatial localization shows a high positional coincidence with the nearby high proper motion K-type star PM J23221-0301. Follow-up X-ray observations confirmed the flux enhancement of the source, while optical spectroscopic monitoring revealed time-variable features, particularly the disappearance of the H α emission line. This X-ray flare is consistent with a characteristic fast-rise-exponential-decay (FRED) light curve, with a rise timescale of 1.4 ks, a decay timescale of 5.7 ks, and a total duration of ~ 7.1 ks. The peak luminosity in the 0.5–4.0 keV energy band reached $\sim 1.3 \times 10^{31}$ erg s⁻¹, with a total energy release of $\sim 9.1 \times 10^{34}$ erg, consistent with the empirical energy correlations observed in magnetic-reconnection-driven stellar flares, as inferred from the multitemperature plasma structure and H α -X-ray energy correlation. This discovery underscores EP's capability in understanding stellar magnetic activity via observing stellar transients.

Keywords: X-ray transient sources, Stellar flare

1. Introduction

Stellar flares are sudden electromagnetic outbursts characterized by rapid radiation enhancement spanning X-ray to radio wavelengths, with typical durations ranging from minutes to hours. Stellar flares are widely observed in late-type stars with spectral types F, G, K, and M. The luminosity of stellar flares is typically in the range 10^{26-33} erg s⁻¹, with total energy on the order of 10^{28-37} erg, and the temperatures reach 10^{6-8} K (Benz and Güdel, 2010). As late-type main-sequence stars, K-type stars exhibit magnetic activity levels significantly higher than G-type stars (e.g., the Sun) but lower than M-type red dwarfs. Recent studies suggest that flare frequency and energy release may profoundly influence the atmospheric escape of their planets (Davenport et al., 2019).

These flares are believed to be caused by the rapid release of magnetic energy during the impulsive reconnection of twisted magnetic fields in the star's outer atmosphere (Shibata and Magara, 2011; Walkowicz et al., 2011). When magnetic field lines

reconnect, nonthermal electrons are accelerated toward the stellar surface, heating the material and causing it to expand into the magnetic loop. This expansion drives a shock wave which propagates along the loop, increasing the density and temperature of the confined plasma (Fisher et al., 1985a,b,c). The plasma then cools through soft X-ray radiation. The density, temperature, and decay time of the flare are directly linked to the geometric properties of the magnetic loop (Reale et al., 2004). For the Sun and other dwarf stars, more luminous flares reach higher temperatures and last longer.

The soft X-ray light curve of flares generally consists of an exponential decay. A gradual rise or a decay composed of segments with different e -folding times can also occur (Osten and Brown, 1999; Reale et al., 2004). The rise phase of a flare typically represents the rapid release of magnetic energy through the magnetic reconnection process, while the decay phase corresponds to the gradual cooling of the flare's source region via thermal conduction and radiative losses (Tsuboi et al., 2016). The flare timescale is often interpreted based on one-dimensional hydrodynamic loop models, in which decay phase reflects the conductive and radiative cooling of confined plasma (Haisch, 1983; Reale, 2003; Reale et al., 2004). However, solar

*E-mail: zhaoyg28@mail2.sysu.edu.cn; shenrf3@mail.sysu.edu.cn

and stellar flares are inherently multi-dimensional phenomena in which multiple loops brighten and evolve successively (Shibata and Magara, 2011). In this context, the overall flare duration can be characterized by the reconnection timescale rather than by the cooling of a single loop. Numerical simulations of multi-thread flare models have demonstrated that the total flare duration scales with the reconnection timescale, largely independent of the detailed cooling processes (Reep and Toriumi, 2017; Namekata et al., 2017).

The $H\alpha$ emission line is the most frequently observed line among solar flare spectroscopic observations (Ichimoto and Kurokawa, 1984) and similar $H\alpha$ line asymmetries to those in solar flares have also been reported during stellar flares (Houdebine et al., 1993; Gunn et al., 1994a,b). Honda et al. (2018) demonstrated that flares lead to a significant enhancement of the $H\alpha$ emission-line strength and emphasized that variations in the $H\alpha$ line profile are associated with the dynamics of cool gas in the flare region. The $H\alpha$ emission-line enhancement typically indicates an energy transport from the corona to the chromosphere during the flare (Mao et al., 2025).

In spite of the substantial progress made in recent years, several fundamental scientific questions in stellar-flare research remain unresolved. First, the physical mechanisms underlying the initiation and energy release of flares, particularly in stars with complex or rapidly evolving magnetic fields, are not yet fully understood. Second, the relationship between stellar flares and associated coronal mass ejections (CMEs) is also poorly constrained, especially for stars beyond the Sun, where direct CME detections remain elusive. Researchers have primarily relied on analyzing plasma motions via Doppler shifts in time-resolved spectroscopy to detect stellar CMEs, yet this method has identified only a few candidates (Chen et al., 2022; Wu et al., 2022; Lu et al., 2022; Namekata et al., 2021). Moreover, how flare properties such as energy, duration, and recurrence rate vary across different stellar types and evolutionary stages remains an open question. Another key challenge lies in characterizing the flare-induced high-energy radiation environment and assessing its cumulative impact on the habitability and atmospheric retention of exoplanets. Addressing these issues requires a combination of high-cadence, multiwavelength observations and advanced theoretical modeling (Vida et al., 2024; Odert et al., 2020; Seli et al., 2025; Hazra et al., 2022; Chen et al., 2021).

Recent studies of stellar flares have utilized the photometric light curve from space surveys, such as the Kepler and K2 missions of the Kepler Space Telescope, and the Transiting Exoplanet Survey Satellite (TESS) (Huber et al., 2014; Günther et al., 2020). The Einstein Probe (EP), launched on 2024 January 9, is dedicated to monitoring the sky in the soft X-ray band (Yuan et al., 2022). Its wide-field X-ray monitoring capabilities have significantly enhanced flare detection efforts, enabling the discovery of an increasing number of stellar flares and thus offer unprecedented opportunities to investigate the energetics and temporal evolution of flares (Yuan et al., 2025).

While numerous stellar flares have been reported from previous missions such as Kepler, TESS and XMM-Newton, EP offers a unique capability through its wide-field X-ray monitoring and rapid follow-up focusing mode, enabling the detection

and characterization of a stellar flare by EP. This event provides a proof-of-concept demonstration of EP’s potential for systematically exploring stellar magnetic activity.

In this paper, we present a comprehensive multiwavelength dataset of the transient EP J2322.1-0301, acquired through a coordinated campaign employing the KAIT photometry and Shane/Kast spectroscopy at Lick Observatory. The paper is structured as follows. We describe the observation and data reduction in Section 2. In Section 3, we analyze the radiation characteristics and temporal evolution of the transient source. Our conclusions are presented in Section 4.

2. Observations and data reduction

Equipped with two scientific instruments, the Wide-field X-ray Telescope (WXT) and the Follow-up X-ray Telescope (FXT), EP offers a large instantaneous field of view for detecting rapid transients, along with a considerable effective area crucial for follow-up observations and precise localization. EP/FXT operates in the 0.5–10.0 keV X-ray band. It consists of two modules (FXT-A and FXT-B), each containing 54 nested Wolter-I paraboloid-hyperboloid mirror shells. The PN-CCD of FXT offers three readout modes, Full Frame mode (FF), Partial Window mode (PW), and Timing mode (TM).

Subsequently, the WXT photon event data processing and calibration pipeline was applied using dedicated data-reduction software coupled with a calibration database system. The extraction and analysis of time-resolved spectra and light curves were conducted utilizing `Fxtsoftv1.05`¹ of the EP data analysis software.

2.1. Einstein Probe Discovery

On September 27, 2024 (UTC), EP-WXT detected a new X-ray transient (trigger ID 01709061302, CMOS36) (Shui et al., 2024), which was designated as EP J2322.1-0301. EP/WXT has a total of 48 detection units (CMOS01-CMOS48), among which CMOS36 and CMOS37 are the two adjacent detection units covering the target sky area in this observation. Since the target is located in the overlapping region of the two units, it is simultaneously detected by CMOS36 and CMOS37. Figure 1 presents the temporal evolution of flares observed by WXT in the 0.5-4.0 keV band, as well as the temporal evolution of flares from the FXT in two energy bands (0.5-2.0 keV and 2.0-10.0 keV), along with the evolution of the FXT hardness ratio. For reference, t_0 denotes the WXT trigger time of 2024-09-27T01:03:48 (UTC). The light curve of this transient exhibits a typical evolutionary pattern of rapid rise and gradual decay. Notably, the decay phase of the flares is relatively prolonged; meanwhile, the FXT hardness ratio shows only minor variations.

The WXT source is positioned at R.A. = 350.551°, Dec. = −3.026°, with an uncertainty of 2.461′. FXT initiated follow-up observations 329 s later, pinpointing the source at R.A. = 350.544°, Dec. = −3.028°, with a positional uncertainty of

¹<http://epfxt.ihep.ac.cn/analysis>

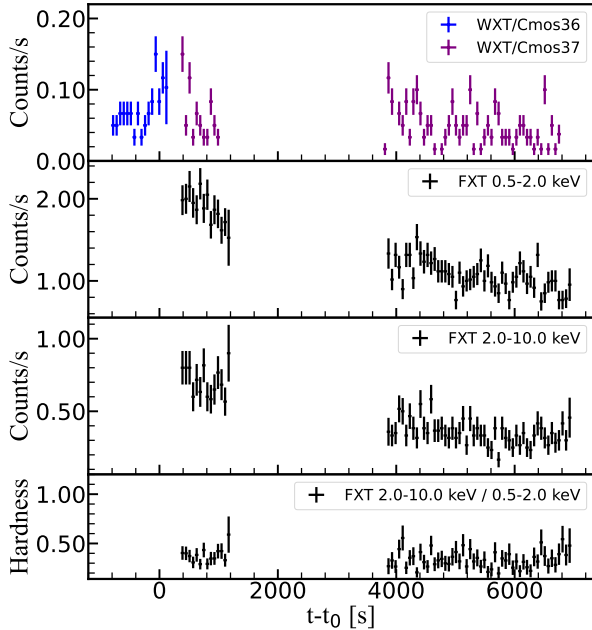


Figure 1: The 60 s time-binned light curves of EP J2322.1-0301, as observed by WXT in the 0.5–4.0 keV band and by the FXT in two energy bands, along with the hardness ratio defined as $C_{2.0-10 \text{ keV}}/C_{0.5-2.0 \text{ keV}}$ (exhibiting only slight variations). Here, t_0 is the WXT trigger time 2024-09-27T01:03:48 (UTC). WXT/CMOS36 and WXT/CMOS37 represent two adjacent CMOS detection units of EP/WXT, and the target is located in the overlapping region of the fields of view of the two units.

$\sim 20''$, consistent with the WXT transient’s location, shown in Figure 2.

Within the WXT error circle, archival data from ROSAT, Gaia DR3, 2MASS, ASAS-SN, WISE, and USNO-B1 were cross-matched. Table 1 presents the cataloged known sources within this region. Additionally, within the FXT error circle, Gaia, 2MASS and ASAS-SN sources are identified, which are associated with the high proper motion star PM J23221-0301 (Gaia Collaboration, 2020). Notably, although other potential counterparts exist within the WXT error circle, all of them are located outside the FXT error circle, exhibiting extremely low association probabilities with the event, compared to PM J23221-0301. This finding strengthens the case for this high proper motion star being the most likely physical host of EP J2322.1-0301.

PM J23221-0301 is located at R.A. = 350.546° , Dec. = -3.029° . Previous ROSAT observations identified it as the X-ray source 1RXS J232210.8-030147, with a quiescent flux of $1.04 \times 10^{-12} \text{ erg s}^{-1} \text{ cm}^{-2}$ (Voges et al., 1999), while ASAS-SN optical monitoring revealed sporadic brightening episodes².

Further constraints on the fundamental stellar properties of PM J23221-0301 are derived from its observed atmospheric

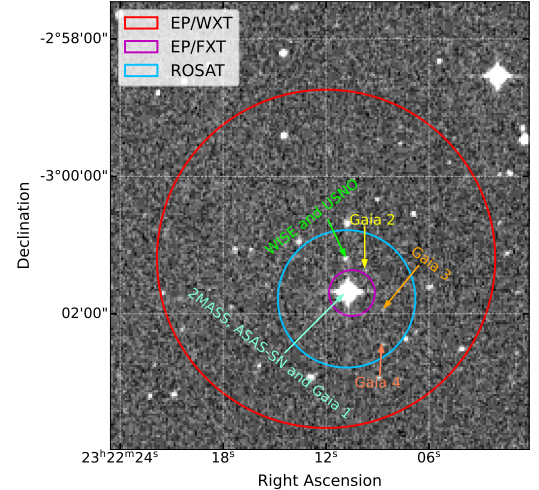


Figure 2: The EP/WXT detection localization (red circle, $2.46'$ error radius), the subsequent EP/FXT refinement (cyan circle, $20''$ radius), and the ROSAT cataloged source localization (blue circle) overlaid on the Digital Sky Survey (DSS) optical image. Potential candidate multiwavelength counterparts within the WXT error circle, including Gaia DR3, 2MASS, WISE, and USNO are also labeled. The high proper motion K-type star PM J23221-0301 is the centrally brighter star indicated by the aquamarine arrow, showing $< 6''$ offset from the FXT centroid.

parameters and archival data. Specifically, SIMBAD³ provides a distance measurement of $46.218 \pm 0.0378 \text{ pc}$ (Steinmetz et al., 2020), a stellar rotation period of 1.28 days (Kiraga and Stepień, 2013) and a stellar age of 1.2 Gyr. The star is of K type with effective temperature $T_{\text{eff}} = 4055 \text{ K}$ (Abdurro’uf et al., 2022). Utilizing the mass-effective temperature scaling relation for K-type main-sequence stars presented in Pecaut and Mamajek (2013), we derive a stellar mass of $M_* \approx 0.70 M_\odot$. Combining this with the measured surface gravity ($\log g = 4.634 \text{ [cgs]}$, Abdurro’uf et al. (2022)), we calculate the stellar radius to be $R_* \approx 0.72 R_\odot$.

2.2. Lick Observatory KAIT Photometry and Kast Spectroscopy

Follow-up photometric observations of PM J23221-0301 within the FXT localization region were conducted using the 0.76 m Katzman Automatic Imaging Telescope (KAIT), as part of the Lick Observatory Supernova Search (LOSS; Filippenko et al. 2001). Observations began $\sim 2 \text{ hr}$ after t_0 and continued over subsequent nights to monitor potential post-flare evolution. The KAIT observations utilized standard B , V , R , and I filters, and additional clear-band images (Li et al., 2011). The resulting optical light curves shown in Figure 3 exhibit no clear evidence of flaring activity, although low-amplitude fluctuations ($\sim 0.2 \text{ mag}$) are present across all photometric bands. This absence of activity may be due to the delayed start of the KAIT observations, which likely missed some prompt activity associated with the initial high-energy transient signal.

²<https://asas-sn.osu.edu/>

³<https://simbad.cds.unistra.fr/simbad/>

Table 1: Cataloged known sources within the WXT localization error circle.

Instruments	Source Name	R.A., Dec.	Distance [pc]	Flux [erg cm ⁻² s ⁻¹]	Magnitude [mag]	Wave Band
2MASS ^a	23221088-0301417	350.543, -3.028	-	-	8.73	Infrared
ASAS-SN ^b	J232211-0301.7	350.545, -3.028	46.2	-	11.42	Optical
Gaia DR3 ^c	2637463382668201856	350.545, -3.028	-	-	10.78	Optical
Gaia DR3 ^c	2637464134287151488	350.541, -3.022	5058.2	-	20.10	Optical
Gaia DR3 ^c	2637464099929200256	350.546, -3.041	364.6	-	20.70	Optical
Gaia DR3 ^c	2637463344013160832	350.536, -3.041	-	-	20.6	Optical
WISE ^d	J232210.94-030110.9	350.546, -3.020	-	-	16.8	Infrared
USNO-B1 ^e	0869-0701355	350.546, -3.020	-	-	20.90	Optical
ROSAT ^f	1RXS J232210.8-030147	350.545, -3.030	53	1.04e-12	-	X-ray

^a Cutri et al. (2003). ^b Kiraga and Stepien (2013). ^c Gaia Collaboration (2022). ^d Cutri et al. (2012). ^e Monet et al. (2003). ^f Voges et al. (1999).

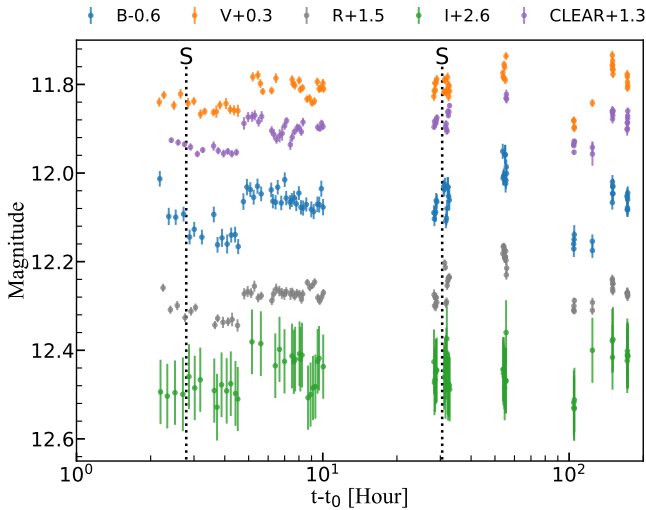


Figure 3: Short-term KAIT optical light curves of PM J23221-0301. The “S” notations and dash lines mark the commencement of Kast’s two spectral observations, corresponding to 2.79 hr and 30.53 hr post-WXT trigger.

Optical spectra of PM J23221-0301 were obtained using the Kast spectrograph on the Shane 3 m telescope at Lick Observatory (Miller et al., 1988). The instrumental resolution is $\sim 18 \text{ \AA}$ at the central wavelength of 6800 \AA . The first epoch observation was conducted on 2024-09-27T03:50:24 ($t_0+2.79 \text{ hr}$), covering a wavelength range of $5800\text{--}7400 \text{ \AA}$ (Zheng et al., 2025). As shown in Figure 4, the spectrum shows a red continuum with narrow absorption lines consistent with a K-type star spectrum. Notably, a strong $H\alpha$ emission line is present, confirming the active nature of PM J23221-0301. The $H\alpha$ line profile in the first epoch is symmetric within the spectral resolution, showing no evident blue- or red-wing asymmetry.

To investigate the temporal evolution of this activity, a second-epoch spectrum was obtained on the following night, ~ 1.272 days after the trigger, covering a broader wavelength range of $3500\text{--}10,000 \text{ \AA}$ (Zheng et al. (2025); see Figure 4). In this spectrum, the $H\alpha$ emission line had nearly disappeared compared to the previous spectrum, confirming PM J23221-0301 as the optical counterpart of the EP flare event.

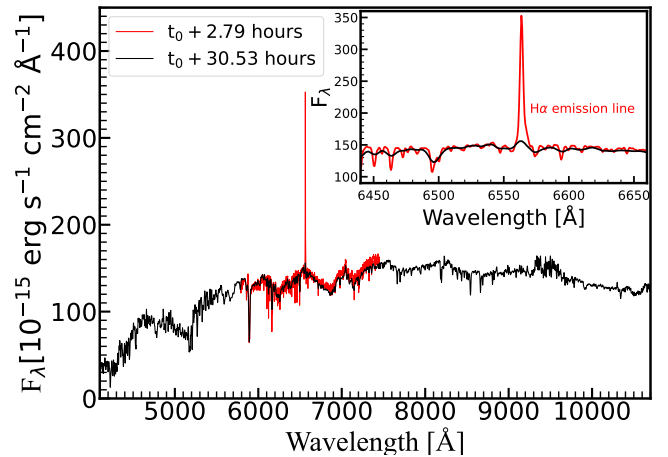


Figure 4: Optical spectra of PM J23221-0301, obtained using Kast on two consecutive nights: 2.79 hr (red) and 30.53 hr (black) post-WXT trigger. Notably, as shown in the zoomed-in panel, the 2.79 hr spectrum features a distinct $H\alpha$ emission line ($\lambda = 6563 \text{ \AA}$); however, this emission line is absent the next night.

2.3. ASAS-SN

PM J23221-0301 is also regularly monitored in the optical by the ASAS-SN project (Shappee et al., 2014). While no significant outburst was detected during the FXT observation window, a relatively small variation in the optical light curve was identified between $t_0 - 1$ and $t_0 + 5$ days, shown in Figure 5. The absence of pronounced optical flaring signatures may be attributed to the temporal resolution limitations of the ASAS-SN monitoring, whose sampling cadence is ~ 1 day. Given the transient nature of the X-ray emission (duration $\sim 7.1 \text{ ks}$), the rapid flux variations could have been averaged out below the optical detection threshold. This likely prevented the capture of any optical counterpart synchronous with the X-ray flare.

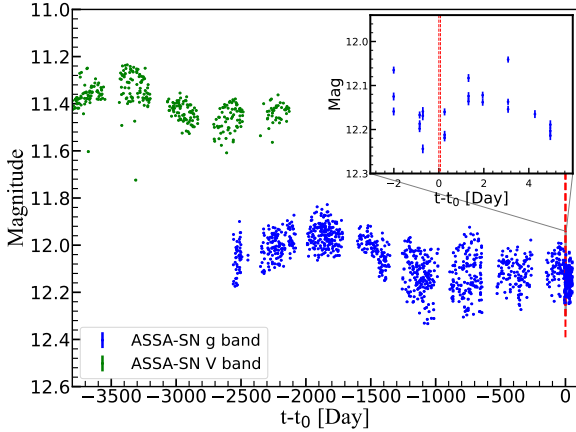


Figure 5: Long-term ASAS-SN optical light curves of PM J23221-0301, with data obtained from <https://asas-sn.osu.edu/>. The red dashed vertical lines demarcate the EP observation window.

3. Spectral and Temporal Analysis

3.1. X-ray Spectral Fitting

Stellar flares are typically emitted from a hot plasma triggered by magnetic reconnection, which exhibit radiation characteristics dominated by thermal continuum emission superimposed with metal-line emission. In X-ray astronomy, the emission from hot plasmas is typically described by the Astrophysical Plasma Emission Code (APEC; Smith et al., 2001) model with two free parameters: the normalization of surface brightness and the temperature. The APEC model accurately simulates the spectral features of thermal plasma by computing ionization equilibrium, atomic transitions, and line-emission processes, making it particularly suited for spectral fitting of hot coronal regions or magnetic loop structures during flares (Smith et al., 2001; Brickhouse and Smith, 2005).

For a hot plasma at an angular distance of D_A to the observer, the observed spectral flux $F(E)$ [$\text{erg cm}^{-2} \text{s}^{-1} \text{keV}^{-1}$] is obtained by integrating over the plasma volume,

$$F(E) = \frac{1}{4\pi[D_A(1+z)]^2} \int_V \Lambda(E, T) dV, \quad (1)$$

where z is the redshift, and $\Lambda(E, T) \propto n_e n_H T^{-1/2} e^{-E/(kT)}$ is the photon emissivity [$\text{erg cm}^{-3} \text{s}^{-1} \text{keV}^{-1}$] for bremsstrahlung (thermal continuum radiation), which depends on the plasma temperature T and photon energy E (n_e and n_H are the electron and hydrogen number densities [cm^{-3}], respectively). For practical use, APEC uses a normalization factor,

$$\text{norm} = \frac{10^{-14}}{4\pi[D_A(1+z)]^2} \int_V n_e n_H dV. \quad (2)$$

We first performed a spectral analysis of the time-integrated FXT data over the entire FXT observation period of $t_0 + (329 \text{ s}, 6929 \text{ s})$ via Xspec⁴. For the spectral model, we ini-

⁴<https://heasarc.gsfc.nasa.gov/xanadu/xspec/manual/manual.html>

tially tried a two-temperature collisional ionization equilibrium model ($\text{tbabs} \times (\text{apec} + \text{apec})$). The first component is responsible for the Galactic absorption using the Tuebingen-Boulder interstellar medium absorption model (Wilms et al., 2000). For the Galactic hydrogen column density, we adopted $N_H = 1.01 \times 10^{16} \text{ cm}^{-2}$, as calculated by Xspec. This model yielded a reduced chi-squared of $\chi^2/\text{dof} = 222.59/133$, with significant residuals observed at low energies (see Figure 6). Table 2 summarizes the results of the fitting and the derived parameters, offering a clearer evaluation of the quality of fitting.

To address this low-energy excess residual in fitting, we introduce an additional thermal component, constructing a three-temperature model ($\text{tbabs} \times (\text{apec} + \text{apec} + \text{apec})$). For the Galactic hydrogen column density, we adopt the value derived from the two-component APEC model fit. The implementation of the three-APEC model significantly improved the fitting quality, yielding $\chi^2/\text{dof} = 143.29/131$, as shown in Table 2, which demonstrates a statistically significant improvement compared to the two-APEC model. This implies the necessity of multi-temperature plasma components to characterize this flare event.

Next, we use the Xselect tool to perform time binning of the WXT and FXT data, respectively, and then extract the spectral data in the 0.5–4.0 keV energy range for each time slice. In the rise phase of the flare, varying time bins were applied to Cmos36 (413 s, 430 s and 117 s), Cmos37 and FXT. Given that the Cmos37 and the FXT observing time periods are mostly overlapping, we jointly fitted the data from the two instruments to obtain more accurate fluxes. During the decay phase, Cmos37 and FXT adopted a $\sim 500 \text{ s}$ time bin to continuously acquire 7 data points. Since these sampling intervals are significantly smaller than the flare’s rise and decay timescales, the flux evolution process was effectively captured. Background subtraction was executed with source-centered annular regions.

We then independently fitted each time slice with the three-temperature APEC model via Xspec software to derive the absorption-corrected X-ray fluxes, with the absorption set to the Galactic value ($N_H = 1.01 \times 10^{16} \text{ cm}^{-2}$). The results are presented in Table 3. The temperature of the hot component varies significantly over time, whereas the temperature of the cool component remains relatively stable throughout the observation period.

3.2. X-ray Light Curve

Finally, based on the time-resolved spectral analysis, we plot the X-ray light curve in Figure 7, with the temperature variation of the hot plasma component shown in the bottom panel. The curve is consistent with a fast-rise-exponential-decay (FRED) profile characterized by a rapid rise and an exponential decay.

To quantify, we adopt the following FRED function to model the X-ray light curve (Osten et al., 2016; Gunther et al., 2020; Sasaki et al., 2021; Mao et al., 2025):

$$F_X(t) = F_{X,q} + \begin{cases} 0, & t < t_{\text{ST}}, \\ (F_{X,\text{peak}} - F_{X,q}) \times \frac{t - t_{\text{ST}}}{t_{\text{peak}} - t_{\text{ST}}}, & t_{\text{ST}} < t < t_{\text{peak}}, \\ (F_{X,\text{peak}} - F_{X,q}) \times \exp\left(-\frac{t - t_{\text{peak}}}{\tau_{\text{decay}}}\right), & t > t_{\text{peak}}, \end{cases} \quad (3)$$

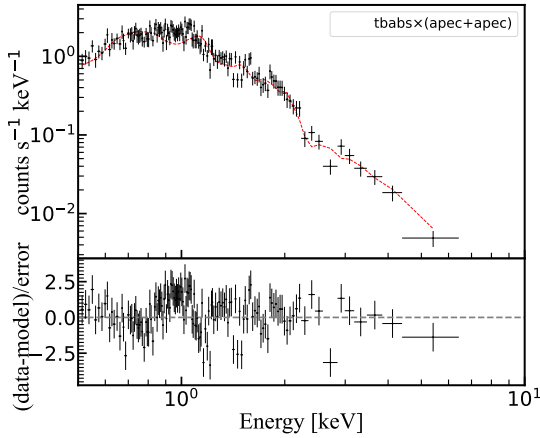
Table 2: Best-fitting parameters for the FXT spectra.

	kT_1	kT_2	kT_3	$F_{0.5-10 \text{ keV}}$	χ^2/dof
	[keV]	[keV]	[keV]	[$10^{-11} \text{ erg s}^{-1} \text{ cm}^{-2}$]	
tbabs \times (apec + apec)	$3.40^{+0.40}_{-0.32}$	$0.32^{+0.03}_{-0.04}$	-	$1.22^{+0.16}_{-0.20}$	222.59/133
tbabs \times (apec + apec + apec)	$4.71^{+1.18}_{-0.73}$	$1.12^{+0.12}_{-0.11}$	$0.27^{+0.03}_{-0.03}$	$1.36^{+0.06}_{-0.01}$	143.29/131

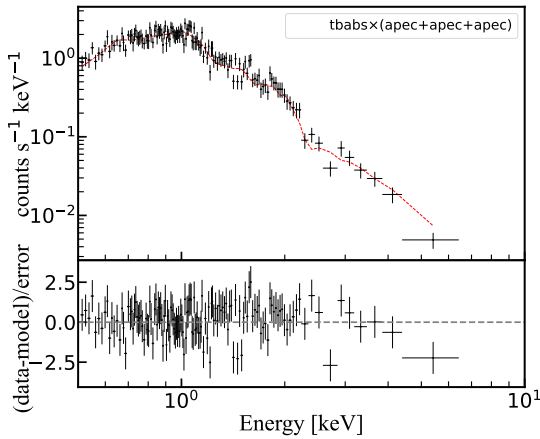
Table 3: Time-resolved spectral fitting results.

Instruments	Time Interval	kT_1	kT_2	kT_3	Flux	χ^2/dof
	[s]	[keV]	[keV]	[keV]	[$10^{-11} \text{ erg cm}^{-2} \text{ s}^{-1}$]	
WXT (cmos36)	(-843, -430)	$6.42^{+1.40}_{-1.13}$	$1.25^{+0.20}_{-0.19}$	$1.07^{+0.10}_{-0.10}$	1.7 ± 0.1	10/9
	(-430, 0)	$6.81^{+2.50}_{-1.90}$	$1.22^{+0.15}_{-0.25}$	$0.87^{+0.21}_{-0.11}$	2.5 ± 0.2	8.8/6
	(0, 117)	$6.96^{+2.21}_{-1.50}$	$1.24^{+0.10}_{-0.10}$	$1.01^{+0.10}_{-0.10}$	4.9 ± 0.5	6.7/4
WXT (cmos37)+FXT	329-659	$6.61^{+1.24}_{-0.92}$	$1.24^{+0.11}_{-0.07}$	$0.27^{+0.01}_{-0.02}$	5.0 ± 0.4	235.5/176
	659-989	$6.85^{+1.01}_{-1.01}$	$1.02^{+0.05}_{-0.05}$	$0.27^{+0.01}_{-0.01}$	4.8 ± 0.2	224/191
	3869-4379	$3.77^{+0.49}_{-0.49}$	$1.48^{+0.15}_{-0.15}$	$0.95^{+0.07}_{-0.03}$	2.7 ± 0.2	250.9/195
	4379-4889	$6.16^{+0.19}_{-0.80}$	$3.60^{+1.32}_{-1.60}$	$0.11^{+0.03}_{-0.03}$	2.5 ± 0.1	176.6/121
	4889-5309	$4.38^{+0.20}_{-0.10}$	$1.39^{+0.21}_{-0.12}$	$0.12^{+0.10}_{-0.10}$	2.4 ± 0.1	147.1/170
	5309-5809	$4.12^{+0.40}_{-0.70}$	$1.60^{+0.89}_{-0.82}$	$0.4^{+0.22}_{-0.12}$	2.1 ± 0.2	172.5/128
	5809-6309	$4.04^{+0.50}_{-0.26}$	$1.03^{+0.60}_{-0.73}$	$0.84^{+0.19}_{-0.12}$	2.0 ± 0.2	146/166
	6309-6749	$5.29^{+0.90}_{-0.32}$	$1.35^{+0.50}_{-0.22}$	$0.98^{+0.39}_{-0.54}$	1.7 ± 0.1	110/82

The averaged absorbed flux is derived in the 0.5–4.0 keV band using the spectra model tbabs \times (APEC+APEC+APEC) for the spectra of WXT(cmos36) and WXT(cmos37)+FXT.



(a)



(b)

Figure 6: Spectral fit of the flare in the 0.5–10.0 keV band from t_0+329 s to t_0+6929 s. The top section of each panel is the observed energy spectrum and the model (red dotted line), while the bottom section shows the residuals. Panel (a) is for a two-APEC model, which exhibits significant residuals at $E \approx 1$ keV. Panel (b), utilizing a three-APEC model with an additional thermal component, effectively improves the fitting quality in the 1 keV region, with residuals notably reduced. This indicates that a multitemperature model can more accurately characterize this flare.

where t denotes the time since the trigger, t_{ST} is the time when the flux starts to increase, t_{peak} is the time when the flux reaches the peak, τ_{decay} is the e -folding time of the decay, $F_{\text{X,peak}}$ is the peak flux, and $F_{\text{X,q}}$ is the non-flaring quiescent level flux. Since the EP observational coverage is not sufficiently long (Figure 1), the count rate and flux lightcurves do not show clearly a quiescent level. Therefore we fix $F_{\text{X,q}}$ to be the historical ROSAT observed flux of 1.04×10^{-12} erg s $^{-1}$ cm $^{-2}$ (Section 2.1 and Table 1). The best-fit model curve is shown as the dashed line in Figure 7. The e -folding decay timescale is constrained to be $\tau_{\text{decay}} \approx 5.7$ ks. The rise time $\tau_{\text{rise}} = t_{\text{peak}} - t_{\text{ST}} \approx 1.4$ ks is derived from the time difference between the flux peak and the start time.

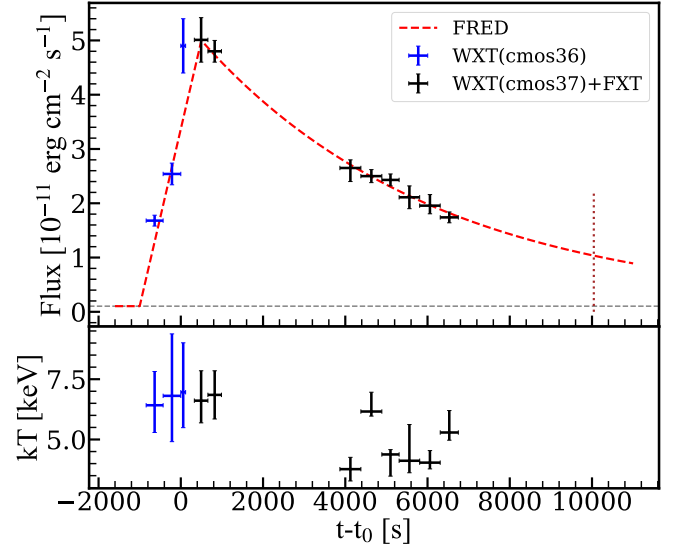


Figure 7: *Top*: temporal modeling of the 0.5–4.0 keV X-ray flare using a FRED model. For the soft X-rays, the unabsorbed flux in the 0.5–4.0 keV band for each spectrum was estimated using the cflux model during spectral fitting in Xspec (see Section 3.1 for the spectral fitting process.). The best-fit FRED model (red dashed line) yields a rise time ($\tau_{\text{rise}} \approx 1.4$ ks) and decay time ($\tau_{\text{decay}} \approx 5.7$ ks). The brown dotted line corresponds to the timing of the first Kast spectral observation. The gray dashed line indicates the quiescent flux during nonflaring periods. *Bottom*: the temperature time variation of the hot plasma component. Note: Figure 7 uses larger bins for unabsorbed flux, while Figure 1 shows 60 s binned count rates.

3.3. Flare Luminosity and Energy

We estimate the total radiated energy E_{X} by integrating the flux over the duration of the flares $E_{\text{X}} = 4\pi d^2 \int F_{\text{X}}(t) dt$, where d is the distance to source which we adopt the reported distance of 46.2 pc for PM J23221-031. We then obtained $E_{\text{X}} = 9.1 \times 10^{34}$ erg. The 0.5–4.0 keV peak flux is $F_{\text{X,peak}} = 5 \times 10^{-11}$ erg s $^{-1}$ cm $^{-2}$, corresponding to a peak X-ray luminosity of $L_{\text{X,peak}} = 1.3 \times 10^{31}$ erg s $^{-1}$.

In Figure 8 we plot the flare peak luminosity versus the flare duration τ , defined as the sum of the rise time τ_{rise} and decay duration τ_{decay} , for EP J2322.1-0301 along with a sample of stellar X-ray flares (Yang et al., 2023; Getman et al., 2021; Pye et al., 2015; Tsuru et al., 1989; Endl et al., 1997; Franciosini et al., 2001; Pandey and Singh, 2012; Tsuboi et al., 2016; Sasaki et al., 2021; Karmakar et al., 2023). Notably, the peak luminosity of EP J2322.1-0301 falls within the main region of the parameter space of previously documented stellar X-ray flares.

3.4. H α Emission

Here we analyze the H α emission in the $t = 2.79$ hr spectrum (Figure 4). The equivalent width (EW) of this spectral feature, $\text{EW} = \int_{\lambda} (F_{\lambda} - F_{\text{cont}})/F_{\text{cont}} d\lambda$, where F_{λ} denotes the wavelength-dependent flux of the emission line and F_{cont} represents the corresponding continuum flux density, is estimated to be 5.07 Å. Then the H α line flux is derived as $F_{\text{H}\alpha} = \text{EW} \times F_{\text{cont}} = 7.6 \times 10^{-13}$ erg s $^{-1}$ cm $^{-2}$.

Note that Namekata et al. (2024) derived an empirical power-law scaling relation between the energies emitted in X-rays

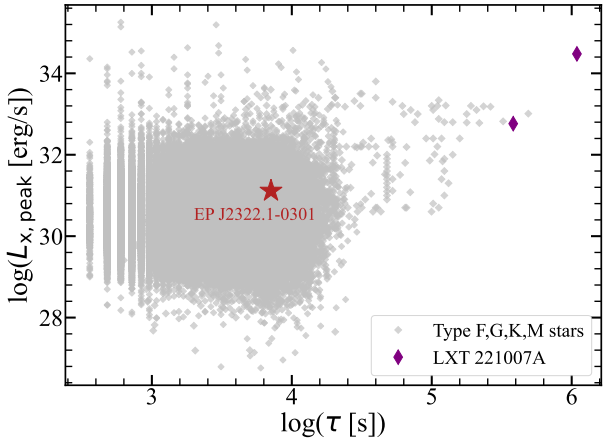


Figure 8: Flare duration versus flare peak luminosity for EP J2322.1-0301 and a sample of stellar X-ray flares. The gray squares are for flares from stars of different spectral types (Yang et al., 2023; Getman et al., 2021; Pye et al., 2015; Tsuru et al., 1989; Endl et al., 1997; Franciosini et al., 2001; Pandey and Singh, 2012; Tsuboi et al., 2016; Sasaki et al., 2021; Karmakar et al., 2023). The two purple diamonds denote the most energetic and longest-duration stellar flare on record, LXT 221007A, corresponding to the main flare and secondary flare, respectively (Mao et al., 2025).

(0.1-100 keV) and $H\alpha$ lines for stellar flares. Here we estimate the energy ratio $E_X/E_{H\alpha}$ for EP J2322.1-0301. The $H\alpha$ spectra of EP J2322.1-0301 were obtained after the peak of the soft X-ray emission, when the flare had entered its decay phase. It has been noted in the literature (Veronig et al., 2002; Doyle et al., 1988; Fuhrmeister et al., 2011; Namekata et al., 2020; Kawai et al., 2022) that for solar & stellar flares both the soft X-ray and $H\alpha$ emissions follow an exponential decay law, and the temporal profiles in the two wavelengths have about the same peak times and the same decay timescales.

Therefore, we estimate the energy ratio to be the flux ratio at the $H\alpha$ observation time: $E_X/E_{H\alpha} = F_X(t = 2.79 \text{ hr})/F_{H\alpha}(t = 2.79 \text{ hr}) = 15.2$. Here to get $F_X(t = 2.79 \text{ hr})$ we have extrapolated from $F_{X,\text{peak}}$ using the best-fit FRED profile (Figure 7). A conversion factor of 1.2 is also included for extrapolating F_X from the 0.5-4.0 keV band to the 0.1-100 keV. This value falls well within the range reported in previous studies, with Kawai et al. (2022) reporting an $E_X/E_{H\alpha} \approx 10$, and Namekata et al. (2024) finding a broader range of 10 to 100.

3.5. Stellar Rotation

The star PM J3221-0301 rotates with a period of 1.28 days (Kiraga and Stepień, 2013). If a flare happens in a region close to the stellar limb, the flaring region may gradually move into the hemisphere facing away from the observer (Stelzer et al., 1999; Güdel et al., 2003; Kowalski, 2024). Such rotational modulation can lead to a gradual decline in the observed emission, and thus may give an apparently shorter decay timescale relative to the intrinsic evolution (Johnstone et al., 2012).

Due to the sparsity of the data coverage, we can not rule out this possibility at working for EP J2322.1-030. Given the rota-

tion period of 1.28 days, at $t_0 + 30.53 \text{ hr}$ the flaring region should have completed nearly a full rotation and reappeared in the observer's line of sight. If the flare were still active at that time, significant $H\alpha$ emission should still be detectable. However, no enhanced $H\alpha$ feature is observed (Figure 4). This indicates that the flare had fully ceased by then. Therefore, we can place an upper limit of 30.53 hr on the intrinsic flare duration, if the observed decay in EP J2322.1-030 were due to the rotational modulation.

4. Conclusion

In this work, we present the discovery and multiwavelength characterization of the X-ray transient EP J2322.1-0301, discovered by the Einstein Probe (EP) on 2024 September 27. We identify it as a stellar flare from the high proper motion K-type star PM J23221-0301. The association with a stellar flare is confirmed by multiple lines of evidence: the spatial coincidence between the X-ray transient and PM J23221-0301 (within $20''$ position uncertainly), the X-ray light curve shape consistent with a FRED profile, the transient $H\alpha$ emission line in optical spectra, and a consistency of flare energetics with known stellar-flare properties.

The FRED-profile fit to the X-ray light curve of EP J2322.1-0301 suggests a rise time $\tau_{\text{rise}} \approx 1.4 \text{ ks}$ and a decay time $\tau_{\text{decay}} \approx 5.7 \text{ ks}$, yielding a total duration of $\sim 7.1 \text{ ks}$. These timescales fall within the typical range of stellar flares reported in the literature (Pye et al., 2015; Tsuru et al., 1989; Endl et al., 1997; Franciosini et al., 2001; Pandey and Singh, 2012; Tsuboi et al., 2016; Liang et al., 2016; Karmakar et al., 2023; Yan et al., 2021).

Optical spectra obtained with the Kast spectrograph at Lick Observatory provide critical evidence for the flare association: a prominent $H\alpha$ emission line detected in the spectrum taken 2.79 hr post-trigger disappeared in the follow-up observation 1.27 days later. The 2-hr time interval between the X-ray peak and the $H\alpha$ detection is significantly shorter than the typical recurrence interval of 10 hr-30 days for stellar flares (Imanishi et al., 1999; Kamio et al., 2003). We therefore consider the probability that the observed $H\alpha$ enhancement is caused by another independent flare to be low, though it cannot be entirely ruled out.

We compare EP J2322.1-0301 with stellar flares observed in known stars, as shown in Figure 8. Its estimated total energy release at a distance of 46.2 pc ($E_X = 9.1 \times 10^{34} \text{ erg}$) falls within the typical range observed for stellar flares. Such a comparison provides valuable context for understanding the scaling relations between stellar-flare energy and duration.

The spectral analysis reveals a multitemperature plasma, which may suggest a possible stratification of the flaring plasma. This finding is consistent with the standard flare-loop models, where chromospheric evaporation generates hotter plasma in the upper regions of the loop and cooler material at lower altitudes (Reale et al., 1997; Reale and Micela, 1998; Fisher et al., 1985a). This inclusion of an additional component resolves the low-energy residuals observed in the two-temperature fit (Figure 6); this supports that a multitemperature

stratified plasma exists in the flare process, reflecting the rapid heating and gradual cooling processes triggered by magnetic reconnection.

Assuming that the temporal evolution of the $H\alpha$ line emission tracks that of the X-rays, we derived the total X-ray-to- $H\alpha$ energy ratio of $E_X/E_{H\alpha} \approx 15.2$, consistent with the empirical X-ray vs. $H\alpha$ relations observed in stellar flares (Kawai et al., 2022; Namekata et al., 2024). We can not rule out a possibility that the observed X-ray decay phase is caused by the star’s rotational modulation to a longer flare that happens close to the stellar limb. If that were the case, we can put an upper limit of 30.53 hr on the intrinsic flare duration (Section 3.5).

This study is one of the early achievements in the synergistic detection of K-type star flares using WXT and FXT of EP. EP identified the transient EP J2322.1-0301 via wide-field monitoring in the 0.5-4.0 keV energy band using WXT, achieving a localization error of only 2.461 arcminutes. Subsequently, FXT performed rapid focusing within 329 s, reducing the localization error to $\sim 20''$, which is crucial for identifying optical counterparts. Ultimately, a precise spatial correlation was established between the X-ray source and the optical star PM J23221-0301, with a position offset of less than 6 arcseconds. This “first detection, then focusing” observational paradigm offers unique advantages for the rapid identification of short-timescale transient flares (e.g., stellar flares) and the investigating their physical associations. It provides a methodological reference for future large-sample statistical studies of stellar flares based on EP. EP’s ability to detect and precisely localize such transient events highlights its capability for studying stellar flares.

Acknowledgements

We thank the referee for valuable comments which improves our manuscript. This work is supported by the National Natural Science Foundation of China (grant NSFC-12393814). C.G. acknowledges support from NSFC grants 12373007 and 12422302. A.V.F.’s research group at UC Berkeley acknowledges financial assistance from the Christopher R. Redlich Fund, Gary and Cynthia Bengier, Clark and Sharon Winslow, Alan Eustace (W.Z. is a Bengier-Winslow-Eustace Specialist in Astronomy), William Draper, Timothy and Melissa Draper, Briggs and Kathleen Wood, Sanford Robertson (T.G.B. is Draper-Wood-Robertson Specialist in Astronomy), and numerous other donors.

KAIT and its ongoing operation were made possible by donations from Sun Microsystems, Inc., the Hewlett-Packard Company, AutoScope Corporation, Lick Observatory, the U.S. NSF, the University of California, the Sylvia&Jim Katzman Foundation, and the TABASGO Foundation. A major upgrade of the Kast spectrograph on the Shane 3 m telescope at Lick Observatory, led by Brad Holden, was made possible through gifts from the Heising-Simons Foundation, William and Marina Kast, and the University of California Observatories. We thank the staff at Lick Observatory for their assistance. Research at Lick Observatory is partially supported by a generous gift from Google.

References

- Abdurro’uf, Accetta, K., Aerts, C., Silva Aguirre, V., Ahumada, R., Ajaonkar, N., Filiz Ak, N., Alam, S., Allende Prieto, C., Almeida, A., Anders, F., Anderson, S.F., Andrews, B.H., Anguiano, B., Aquino-Ortíz, E., Aragón-Salamanca, A., Argudo-Fernández, M., Ata, M., Aubert, M., Avila-Reese, V., Badenes, C., Barbá, R.H., Barger, K., Barrera-Ballesteros, J.K., Beaton, R.L., Beers, T.C., Belfiore, F., Bender, C.F., Bernardi, M., Bershady, M.A., Beutler, F., Bidin, C.M., Bird, J.C., Bizyaev, D., Blanc, G.A., Blanton, M.R., Boardman, N.F., Bolton, A.S., Boquien, M., Borissova, J., Bovy, J., Brandt, W.N., Brown, J., Brownstein, J.R., Brusa, M., Buchner, J., Bundy, K., Burchett, J.N., Bureau, M., Burgasser, A., Cabang, T.K., Campbell, S., Cappellari, M., Carlberg, J.K., Wanderley, F.C., Carrera, R., Cash, J., Chen, Y.P., Chen, W.H., Cherinka, B., Chiappini, C., Choi, P.D., Chojnowski, S.D., Chung, H., Clerc, N., Cohen, R.E., Comerford, J.M., Comparat, J., da Costa, L., Covey, K., Crane, J.D., Cruz-Gonzalez, I., Culhane, C., Cunha, K., Dai, Y.S., Damke, G., Darling, J., Davidson, Jr., J.W., Davies, R., Dawson, K., De Lee, N., Diamond-Stanic, A.M., Cano-Díaz, M., Sánchez, H.D., Donor, J., Duckworth, C., Dwelly, T., Eisenstein, D.J., Elsworth, Y.P., Emsellem, E., Eracleous, M., Escoffier, S., Fan, X., Farr, E., Feng, S., Fernández-Trincado, J.G., Feuillet, D., Filipp, A., Fillingham, S.P., Frinchaboy, P.M., Fromenteau, S., Galbany, L., García, R.A., García-Hernández, D.A., Ge, J., Geisler, D., Gelfand, J., Géron, T., Gibson, B.J., Goddy, J., Godoy-Rivera, D., Grabowski, K., Green, P.J., Greener, M., Grier, C.J., Griffith, E., Guo, H., Guy, J., Hadjara, M., Harding, P., Hasselquist, S., Hayes, C.R., Hearty, F., Hernández, J., Hill, L., Hogg, D.W., Holtzman, J.A., Horta, D., Hsieh, B.C., Hsu, C.H., Hsu, Y.H., Huber, D., Huertas-Company, M., Hutchinson, B., Hwang, H.S., Ibarra-Medel, H.J., Chitham, J.I., Ilha, G.S., Imig, J., Jaekle, W., Jayasinghe, T., Ji, X., Johnson, J.A., Jones, A., Jönsson, H., Katkov, I., Khalatyan, Dr., A., Kinemuchi, K., Kisku, S., Knapen, J.H., Kneib, J.P., Kollmeier, J.A., Kong, M., Kounkel, M., Kreckel, K., Krishnarao, D., Lacerna, I., Lane, R.R., Langgin, R., Lavender, R., Law, D.R., Lazarz, D., Leung, H.W., Leung, H.H., Lewis, H.M., Li, C., Li, R., Lian, J., Liang, F.H., Lin, L., Lin, Y.T., Lin, S., Lintott, C., Long, D., Longa-Peña, P., López-Cobá, C., Lu, S., Lundgren, B.F., Luo, Y., Mackereth, J.T., de la Macorra, A., Mahadevan, S., Majewski, S.R., Machado, A., Mandeville, T., Maraston, C., Margalef-Bentabol, B., Masseron, T., Masters, K.L., Mathur, S., McDermid, R.M., McKay, M., Merloni, A., Merrifield, M., Meszaros, S., Miglio, A., Di Mille, F., Minniti, D., Minsley, R., Monachesi, A., 2022. The Seventeenth Data Release of the Sloan Digital Sky Surveys: Complete Release of MaNGA, MaStar, and APOGEE-2 Data. *ApJS* 259, 35. doi:10.3847/1538-4365/ac4414, arXiv:2112.02026.
- Benz, A.O., Güdel, M., 2010. Physical Processes in Magnetically Driven Flares on the Sun, Stars, and Young Stellar Objects. *ARA&A* 48, 241–287. doi:10.1146/annurev-astro-082708-101757.

- Brickhouse, N.S., Smith, R.K., 2005. Spectral Modeling with APEC. *Highlights of Astronomy* 13, 651. URL: <https://ui.adsabs.harvard.edu/abs/2005HiA...13..651B>.
- Chen, H., Tian, H., Li, H., Wang, J., Lu, H., Xu, Y., Hou, Z., Wu, Y., 2022. Detection of Flare-induced Plasma Flows in the Corona of EV Lac with X-Ray Spectroscopy. *ApJ* 933, 92. doi:10.3847/1538-4357/ac739b, [arXiv:2205.14293](https://arxiv.org/abs/2205.14293).
- Chen, H., Zhan, Z., Youngblood, A., Wolf, E.T., Feinstein, A.D., Horton, D.E., 2021. Persistence of flare-driven atmospheric chemistry on rocky habitable zone worlds. *Nature Astronomy* 5, 298–310. doi:10.1038/s41550-020-01264-1, [arXiv:2101.04507](https://arxiv.org/abs/2101.04507).
- Cutri, R.M., Skrutskie, M.F., van Dyk, S., Beichman, C.A., Carpenter, J.M., Chester, T., Cambresy, L., Evans, T., Fowler, J., Gizis, J., Howard, E., Huchra, J., Jarrett, T., Kopan, E.L., Kirkpatrick, J.D., Light, R.M., Marsh, K.A., McCallon, H., Schneider, S., Stiening, R., Sykes, M., Weinberg, M., Wheaton, W.A., Wheelock, S., Zacarias, N., 2003. VizieR Online Data Catalog: 2MASS All-Sky Catalog of Point Sources (Cutri+ 2003). VizieR On-line Data Catalog: II/246. Originally published in: University of Massachusetts and Infrared Processing and Analysis Center, (IPAC/California Institute of Technology) (2003).
- Cutri, R.M., Wright, E.L., Conrow, T., Bauer, J., Benford, D., Brandenburg, H., Dailey, J., Eisenhardt, P.R.M., Evans, T., Fajardo-Acosta, S., Fowler, J., Gelino, C., Grillmair, C., Harbut, M., Hoffman, D., Jarrett, T., Kirkpatrick, J.D., Leisawitz, D., Liu, W., Mainzer, A., Marsh, K., Masci, F., McCallon, H., Padgett, D., Ressler, M.E., Royer, D., Skrutskie, M.F., Stanford, S.A., Wyatt, P.L., Tholen, D., Tsai, C.W., Wachter, S., Wheelock, S.L., Yan, L., Alles, R., Beck, R., Grav, T., Masiero, J., McCollum, B., McGehee, P., Papin, M., Wittman, M., 2012. Explanatory Supplement to the WISE All-Sky Data Release Products. Explanatory Supplement to the WISE All-Sky Data Release Products.
- Davenport, J.R.A., Covey, K.R., Clarke, R.W., Boeck, A.C., Cornet, J., Hawley, S.L., 2019. The Evolution of Flare Activity with Stellar Age. *ApJ* 871, 241. doi:10.3847/1538-4357/aafb76, [arXiv:1901.00890](https://arxiv.org/abs/1901.00890).
- Doyle, J.G., Butler, C.J., Bryne, P.B., van den Oord, G.H.J., 1988. Rotational modulation and flares on RS CVn and BY Dra systems. VII. simultaneous X-ray, radio and optical data for the dMe star YZ CMi on 4/5 March 1985. *A&A* 193, 229–247.
- Endl, M., Strassmeier, K.G., Kurster, M., 1997. A large X-ray flare on HU Virginis. *A&A* 328, 565–570. URL: <https://ui.adsabs.harvard.edu/abs/1997A&A...328..565E>.
- Filippenko, A.V., Li, W.D., Treffers, R.R., Modjaz, M., 2001. The Lick Observatory Supernova Search with the Katzman Automatic Imaging Telescope, in: Paczynski, B., Chen, W.P., Lemme, C. (Eds.), *IAU Colloq. 183: Small Telescope Astronomy on Global Scales*, p. 121.
- Fisher, G.H., Canfield, R.C., McClymont, A.N., 1985a. Flare loop radiative hydrodynamics. V. Response to thick-target heating. *ApJ* 289, 414–424. doi:10.1086/162901.
- Fisher, G.H., Canfield, R.C., McClymont, A.N., 1985b. Flare Loop Radiative Hydrodynamics. VI. Chromospheric Evaporation due to Heating by Nonthermal Electrons. *ApJ* 289, 425–433. doi:10.1086/162902.
- Fisher, G.H., Canfield, R.C., McClymont, A.N., 1985c. Flare Loop Radiative Hydrodynamics. VII. Dynamics of the Thick Target Heated Chromosphere. *ApJ* 289, 434. doi:10.1086/162903.
- Franciosini, E., Pallavicini, R., Tagliaferri, G., 2001. BeppoSAX observation of a large long-duration X-ray flare from UX Arietis. *A&A* 375, 196–204. doi:10.1051/0004-6361:20010830.
- Fuhrmeister, B., Lalitha, S., Poppenhaeger, K., Rudolf, N., Liefke, C., Reiners, A., Schmitt, J.H.M.M., Ness, J.U., 2011. Multi-wavelength observations of Proxima Centauri. *A&A* 534, A133. doi:10.1051/0004-6361/201117447, [arXiv:1109.1130](https://arxiv.org/abs/1109.1130).
- Gaia Collaboration, 2020. VizieR Online Data Catalog: Gaia EDR3 (Gaia Collaboration, 2020). VizieR On-line Data Catalog: I/350. Originally published in: 2021A&A...649A...1G. doi:10.26093/cds/vizier.1350.
- Gaia Collaboration, 2022. VizieR Online Data Catalog: Gaia DR3 Part 1. Main source (Gaia Collaboration, 2022). VizieR On-line Data Catalog: I/355. Originally published in: doi:10.1051/0004-63. doi:10.26093/cds/vizier.1355.
- Getman, K.V., Feigelson, E.D., Garmire, G.P., 2021. X-Ray Superflares from Pre-main-sequence Stars: Flare Modeling. *ApJ* 920, 154. doi:10.3847/1538-4357/ac1746, [arXiv:2106.08262](https://arxiv.org/abs/2106.08262).
- Güdel, M., Audard, M., Kashyap, V.L., Drake, J.J., Guinan, E.F., 2003. Are Coronae of Magnetically Active Stars Heated by Flares? II. Extreme Ultraviolet and X-Ray Flare Statistics and the Differential Emission Measure Distribution. *ApJ* 582, 423–442. doi:10.1086/344614, [arXiv:astro-ph/0209075](https://arxiv.org/abs/astro-ph/0209075).
- Gunn, A.G., Doyle, J.G., Mathioudakis, M., Avgoloupis, S., 1994a. An optical flare on YZ Canis Minoris. *A&A* 285, 157–160.
- Gunn, A.G., Doyle, J.G., Mathioudakis, M., Houdebine, E.R., Avgoloupis, S., 1994b. High-velocity evaporation during a flare on AT Microscopii. *A&A* 285, 489–496.
- Günther, M.N., Zhan, Z., Seager, S., Rimmer, P.B., Ranjan, S., Stassun, K.G., Oelkers, R.J., Daylan, T., Newton, E., Kristiansen, M.H., Olah, K., Gillen, E., Rappaport, S., Ricker,

- G.R., Vanderspek, R.K., Latham, D.W., Winn, J.N., Jenkins, J.M., Glidden, A., Fausnaugh, M., Levine, A.M., Dittmann, J.A., Quinn, S.N., Krishnamurthy, A., Ting, E.B., 2020. Stellar Flares from the First TESS Data Release: Exploring a New Sample of M Dwarfs. *AJ* 159, 60. doi:[10.3847/1538-3881/ab5d3a](https://doi.org/10.3847/1538-3881/ab5d3a), [arXiv:1901.00443](https://arxiv.org/abs/1901.00443).
- Gunther, M.N., Zhan, Z., Seager, S., Rimmer, P.B., Ranjan, S., Stassun, K.G., Oelkers, R.J., Daylan, T., Newton, E., Kristiansen, M.H., Olah, K., Gillen, E., Rappaport, S., Ricker, G.R., Vanderspek, R.K., Latham, D.W., Winn, J.N., Jenkins, J.M., Glidden, A., Fausnaugh, M., Levine, A.M., Dittmann, J.A., Quinn, S.N., Krishnamurthy, A., Ting, E.B., 2020. VizieR Online Data Catalog: 8695 flares from 1228 stars in TESS sectors 1 & 2 (Gunther+, 2020). VizieR On-line Data Catalog: J/AJ/159/60. Originally published in: 2020AJ....159...60G. doi:[10.26093/cds/vizier.51590060](https://doi.org/10.26093/cds/vizier.51590060).
- Haisch, B.M., 1983. X-ray observations of stellar flares, in: Byrne, P.B., Rodono, M. (Eds.), *IAU Colloq. 71: Activity in Red-Dwarf Stars*, pp. 255–268. doi:[10.1007/978-94-009-7157-8_32](https://doi.org/10.1007/978-94-009-7157-8_32).
- Hazra, G., Vidotto, A.A., Carolan, S., Villarreal D'Angelo, C., Manchester, W., 2022. The impact of coronal mass ejections and flares on the atmosphere of the hot Jupiter HD189733b. *MNRAS* 509, 5858–5871. doi:[10.1093/mnras/stab3271](https://doi.org/10.1093/mnras/stab3271), [arXiv:2111.04531](https://arxiv.org/abs/2111.04531).
- Honda, S., Notsu, Y., Namekata, K., Notsu, S., Maehara, H., Ikuta, K., Nogami, D., Shibata, K., 2018. Time-resolved spectroscopic observations of an M-dwarf flare star EV Lacertae during a flare. *PASJ* 70, 62. doi:[10.1093/pasj/psy055](https://doi.org/10.1093/pasj/psy055), [arXiv:1804.03771](https://arxiv.org/abs/1804.03771).
- Houdebine, E.R., Foing, B.H., Doyle, J.G., Rodono, M., 1993. Dynamics of flares on late type dMe stars. II. Mass motions and prominence oscillations during a flare on AD Leonis. *A&A* 274, 245–264.
- Huber, D., Silva Aguirre, V., Matthews, J.M., Pinsonneault, M.H., Gaidos, E., García, R.A., Hekker, S., Mathur, S., Mosser, B., Torres, G., Bastien, F.A., Basu, S., Bedding, T.R., Chaplin, W.J., Demory, B.O., Fleming, S.W., Guo, Z., Mann, A.W., Rowe, J.F., Serenelli, A.M., Smith, M.A., Stello, D., 2014. Revised Stellar Properties of Kepler Targets for the Quarter 1-16 Transit Detection Run. *ApJS* 211, 2. doi:[10.1088/0067-0049/211/1/2](https://doi.org/10.1088/0067-0049/211/1/2), [arXiv:1312.0662](https://arxiv.org/abs/1312.0662).
- Ichimoto, K., Kurokawa, H., 1984. $H\alpha$ Red Asymmetry of Solar Flares. *Sol. Phys.* 93, 105–121. doi:[10.1007/BF00156656](https://doi.org/10.1007/BF00156656).
- Imanishi, K., Tsuboi, Y., Koyama, K., Grosso, N., Montmerle, T., 1999. Quasi-Periodic X-Ray Flares from the Class I Protostar YLW15, in: Nakamoto, T. (Ed.), *Star Formation 1999*, pp. 312–313.
- Johnstone, C.P., Gregory, S.G., Jardine, M.M., Getman, K.V., 2012. The soft X-ray light curves of partially eclipsed stellar flares. *MNRAS* 419, 29–38. doi:[10.1111/j.1365-2966.2011.19666.x](https://doi.org/10.1111/j.1365-2966.2011.19666.x), [arXiv:1108.3999](https://arxiv.org/abs/1108.3999).
- Kamio, S., Kurokawa, H., Ishii, T.T., 2003. Precise determination of cooling times of post-flare loops from the detailed comparison between $H\alpha$ and soft X-ray images. *Sol. Phys.* 215, 127–146. doi:[10.1023/A:1024839732106](https://doi.org/10.1023/A:1024839732106).
- Karmakar, S., Naik, S., Pandey, J.C., Savanov, I.S., 2023. Swift and XMM-Newton observations of an RS CVn-type eclipsing binary SZ Psc: superflare and coronal properties. *MNRAS* 518, 900–918. doi:[10.1093/mnras/stac2970](https://doi.org/10.1093/mnras/stac2970), [arXiv:2210.07170](https://arxiv.org/abs/2210.07170).
- Kawai, H., Tsuboi, Y., Iwakiri, W.B., Maeda, Y., Katsuda, S., Sasaki, R., Kohara, J., MAXI TEAM, 2022. X-ray/ $H\alpha$ scaling relationships in stellar flares. *PASJ* 74, 477–487. doi:[10.1093/pasj/psac008](https://doi.org/10.1093/pasj/psac008), [arXiv:2307.01469](https://arxiv.org/abs/2307.01469).
- Kiraga, M., Stepień, K., 2013. VizieR Online Data Catalog: ASAS photometry of ROSAT sources. II. (Kiraga+, 2013). VizieR On-line Data Catalog: J/AcA/63/53. Originally published in: 2013AcA....63...53K.
- Kiraga, M., Stepień, K., 2013. ASAS Photometry of ROSAT Sources. II. New Variables from the ASAS North Survey. *Acta Astronomica* 63, 53–66. doi:[10.48550/arXiv.1304.3236](https://doi.org/10.48550/arXiv.1304.3236), [arXiv:1304.3236](https://arxiv.org/abs/1304.3236).
- Kowalski, A.F., 2024. Stellar flares. *Living Reviews in Solar Physics* 21, 1. doi:[10.1007/s41116-024-00039-4](https://doi.org/10.1007/s41116-024-00039-4), [arXiv:2402.07885](https://arxiv.org/abs/2402.07885).
- Li, W., Leaman, J., Chornock, R., Filippenko, A.V., Poznanski, D., Ganeshalingam, M., Wang, X., Modjaz, M., Jha, S., Foley, R.J., Smith, N., 2011. Nearby supernova rates from the Lick Observatory Supernova Search - II. The observed luminosity functions and fractions of supernovae in a complete sample. *MNRAS* 412, 1441–1472. doi:[10.1111/j.1365-2966.2011.18160.x](https://doi.org/10.1111/j.1365-2966.2011.18160.x), [arXiv:1006.4612](https://arxiv.org/abs/1006.4612).
- Liang, E.S., Wang, S., Zhou, J.L., Zhou, X., Zhang, H., Xie, J., Liu, H., Wang, L., Ashley, M.C.B., 2016. Stellar Flares in the CSTAR Field: Results from the 2008 Data Set. *AJ* 152, 168. doi:[10.3847/0004-6256/152/6/168](https://doi.org/10.3847/0004-6256/152/6/168), [arXiv:1608.07904](https://arxiv.org/abs/1608.07904).
- Lu, H.p., Tian, H., Zhang, L.y., Karoff, C., Chen, H.c., Shi, J.r., Hou, Z.y., Chen, Y.j., Xu, Y., Wu, Y.c., Cao, D.t., Wang, J.t., 2022. Possible detection of coronal mass ejections on late-type main-sequence stars in LAMOST medium-resolution spectra. *A&A* 663, A140. doi:[10.1051/0004-6361/202142909](https://doi.org/10.1051/0004-6361/202142909), [arXiv:2205.09972](https://arxiv.org/abs/2205.09972).
- Mao, X., Liu, H.Y., Wang, S., Ling, Z., Yuan, W., Cheng, H., Pan, H., Li, D., Favata, F., Ji, T., Zhang, J., Zhao, X., Wang, J., Liu, M., Liu, Y., Cai, Z., Castro-Tirado, A.J., Dai, Y., Deng, L., Ding, X., Ji, K., Jin, C., Lei, Y., Li, H., Lin, J., Liu,

- H., Liu, S., Sun, H., Sun, S., Sun, X., Shi, J., Wang, J., Wang, J., Wang, W., Wei, J., Xin, L., Xiong, D., Zhang, C., Zhang, W., Zhang, Y., Zhang, X., Zhao, D., Zhou, G., 2025. LEIA Discovery of the Longest-lasting and Most Energetic Stellar X-Ray Flare Ever Detected. *ApJ* 980, 268. doi:[10.3847/1538-4357/ada698](https://doi.org/10.3847/1538-4357/ada698), [arXiv:2410.17999](https://arxiv.org/abs/2410.17999).
- Miller, J.S., Robinson, L.B., Goodrich, R.W., 1988. A CCD Spectropolarimeter for the Lick Observatory 3-Meter Telescope, in: Robinson, L.B. (Ed.), *Instrumentation for Ground-Based Optical Astronomy*, p. 157. URL: <https://ui.adsabs.harvard.edu/abs/1988igbo.conf..157M>.
- Monet, D.G., Levine, S.E., Canzian, B., Ables, H.D., Bird, A.R., Dahn, C.C., Guetter, H.H., Harris, H.C., Henden, A.A., Leggett, S.K., Levison, H.F., Luginbuhl, C.B., Martini, J., Monet, A.K.B., Munn, J.A., Pier, J.R., Rhodes, A.R., Riepe, B., Sell, S., Stone, R.C., Vrba, F.J., Walker, R.L., Westerhout, G., Brucato, R.J., Reid, I.N., Schoening, W., Hartley, M., Read, M.A., Tritton, S.B., 2003. The USNO-B Catalog. *AJ* 125, 984–993. doi:[10.1086/345888](https://doi.org/10.1086/345888), [arXiv:astro-ph/0210694](https://arxiv.org/abs/astro-ph/0210694).
- Namekata, K., Airapetian, V.S., Petit, P., Maehara, H., Ikuta, K., Inoue, S., Notsu, Y., Paudel, R.R., Arzoumanian, Z., Avramova-Boncheva, A.A., Gendreau, K., Jeffers, S.V., Marsden, S., Morin, J., Neiner, C., Vidotto, A.A., Shibata, K., 2024. Multiwavelength Campaign Observations of a Young Solar-type Star, EK Draconis. I. Discovery of Prominence Eruptions Associated with Superflares. *ApJ* 961, 23. doi:[10.3847/1538-4357/ad0b7c](https://doi.org/10.3847/1538-4357/ad0b7c), [arXiv:2311.07380](https://arxiv.org/abs/2311.07380).
- Namekata, K., Maehara, H., Honda, S., Notsu, Y., Okamoto, S., Takahashi, J., Takayama, M., Ohshima, T., Saito, T., Katoh, N., Tozuka, M., Murata, K.L., Ogawa, F., Niwano, M., Adachi, R., Oeda, M., Shiraishi, K., Isogai, K., Seki, D., Ishii, T.T., Ichimoto, K., Nogami, D., Shibata, K., 2021. Probable detection of an eruptive filament from a superflare on a solar-type star. *Nature Astronomy* 6, 241–248. doi:[10.1038/s41550-021-01532-8](https://doi.org/10.1038/s41550-021-01532-8), [arXiv:2112.04808](https://arxiv.org/abs/2112.04808).
- Namekata, K., Maehara, H., Sasaki, R., Kawai, H., Notsu, Y., Kowalski, A.F., Allred, J.C., Iwakiri, W., Tsuboi, Y., Murata, K.L., Niwano, M., Shiraishi, K., Adachi, R., Iida, K., Oeda, M., Honda, S., Tozuka, M., Katoh, N., Onozato, H., Okamoto, S., Isogai, K., Kimura, M., Kojiguchi, N., Wakamatsu, Y., Tampo, Y., Nogami, D., Shibata, K., 2020. Optical and X-ray observations of stellar flares on an active M dwarf AD Leonis with the Seimei Telescope, SCAT, NICER, and OISTER. *PASJ* 72, 68. doi:[10.1093/pasj/psaa051](https://doi.org/10.1093/pasj/psaa051), [arXiv:2005.04336](https://arxiv.org/abs/2005.04336).
- Namekata, K., Sakaue, T., Watanabe, K., Asai, A., Maehara, H., Notsu, Y., Notsu, S., Honda, S., Ishii, T.T., Ikuta, K., Nogami, D., Shibata, K., 2017. Statistical Studies of Solar White-light Flares and Comparisons with Superflares on Solar-type Stars. *ApJ* 851, 91. doi:[10.3847/1538-4357/aa9b34](https://doi.org/10.3847/1538-4357/aa9b34), [arXiv:1710.11325](https://arxiv.org/abs/1710.11325).
- Odert, P., Leitzinger, M., Guenther, E.W., Heinzel, P., 2020. Stellar coronal mass ejections - II. Constraints from spectroscopic observations. *MNRAS* 494, 3766–3783. doi:[10.1093/mnras/staa1021](https://doi.org/10.1093/mnras/staa1021), [arXiv:2004.04063](https://arxiv.org/abs/2004.04063).
- Osten, R.A., Brown, A., 1999. Extreme Ultraviolet Explorer Photometry of RS Canum Venaticorum Systems: Four Flaring Megaseconds. *ApJ* 515, 746–761. doi:[10.1086/307034](https://doi.org/10.1086/307034).
- Osten, R.A., Kowalski, A., Drake, S.A., Krimm, H., Page, K., Gazeas, K., Kennea, J., Oates, S., Page, M., de Miguel, E., Novák, R., Apeltauer, T., Gehrels, N., 2016. A Very Bright, Very Hot, and Very Long Flaring Event from the M Dwarf Binary System DG CVn. *ApJ* 832, 174. doi:[10.3847/0004-637X/832/2/174](https://doi.org/10.3847/0004-637X/832/2/174), [arXiv:1609.04674](https://arxiv.org/abs/1609.04674).
- Pandey, J.C., Singh, K.P., 2012. A study of X-ray flares - II. RS CVn-type binaries. *MNRAS* 419, 1219–1237. doi:[10.1111/j.1365-2966.2011.19776.x](https://doi.org/10.1111/j.1365-2966.2011.19776.x), [arXiv:1110.2008](https://arxiv.org/abs/1110.2008).
- Pecaut, M.J., Mamajek, E.E., 2013. Intrinsic Colors, Temperatures, and Bolometric Corrections of Pre-main-sequence Stars. *ApJS* 208, 9. doi:[10.1088/0067-0049/208/1/9](https://doi.org/10.1088/0067-0049/208/1/9), [arXiv:1307.2657](https://arxiv.org/abs/1307.2657).
- Pye, J.P., Rosen, S., Fyfe, D., Schröder, A.C., 2015. A survey of stellar X-ray flares from the XMM-Newton serendipitous source catalogue: HIPPARCOS-Tycho cool stars. *A&A* 581, A28. doi:[10.1051/0004-6361/201526217](https://doi.org/10.1051/0004-6361/201526217), [arXiv:1506.05289](https://arxiv.org/abs/1506.05289).
- Reale, F., 2003. Modeling solar and stellar flares. *Advances in Space Research* 32, 1057–1066. doi:[10.1016/S0273-1177\(03\)00309-0](https://doi.org/10.1016/S0273-1177(03)00309-0).
- Reale, F., Betta, R., Peres, G., Serio, S., McTiernan, J., 1997. Determination of the length of coronal loops from the decay of X-ray flares I. Solar flares observed with YOHKOH SXT. *A&A* 325, 782–790.
- Reale, F., Güdel, M., Peres, G., Audard, M., 2004. Modeling an X-ray flare on Proxima Centauri: Evidence of two flaring loop components and of two heating mechanisms at work. *A&A* 416, 733–747. doi:[10.1051/0004-6361:20034027](https://doi.org/10.1051/0004-6361:20034027), [arXiv:astro-ph/0312267](https://arxiv.org/abs/astro-ph/0312267).
- Reale, F., Micela, G., 1998. Determination of the length of coronal loops from the decay of X-ray flares. II. Stellar flares observed with ROSAT/PSPC. *A&A* 334, 1028–1036.
- Reep, J.W., Toriumi, S., 2017. The Direct Relation between the Duration of Magnetic Reconnection and the Evolution of GOES Light Curves in Solar Flares. *ApJ* 851, 4. doi:[10.3847/1538-4357/aa96fe](https://doi.org/10.3847/1538-4357/aa96fe), [arXiv:1711.00422](https://arxiv.org/abs/1711.00422).
- Sasaki, R., Tsuboi, Y., Iwakiri, W., Nakahira, S., Maeda, Y., Gendreau, K., Corcoran, M.F., Hamaguchi, K., Arzoumanian, Z., Markwardt, C.B., Enoto, T., Sato, T., Kawai, H., Mihara, T., Shidatsu, M., Negoro, H., Serino, M., 2021. The RS CVn-type Star GT Mus Shows Most Energetic X-Ray

- Flares Throughout the 2010s. *ApJ* 910, 25. doi:[10.3847/1538-4357/abde38](https://doi.org/10.3847/1538-4357/abde38), [arXiv:2103.16822](https://arxiv.org/abs/2103.16822).
- Seli, B., Vida, K., Oláh, K., Görgei, A., Soós, S., Pál, A., Kriskovics, L., Kővári, Z., 2025. Stellar flare morphology with TESS across the main sequence. *A&A* 694, A161. doi:[10.1051/0004-6361/202452489](https://doi.org/10.1051/0004-6361/202452489), [arXiv:2412.12989](https://arxiv.org/abs/2412.12989).
- Shappee, B.J., Prieto, J.L., Grupe, D., Kochanek, C.S., Stanek, K.Z., De Rosa, G., Mathur, S., Zu, Y., Peterson, B.M., Pogge, R.W., Komossa, S., Im, M., Jencson, J., Holoiien, T.W.S., Basu, U., Beacom, J.F., Szczygieł, D.M., Brimacombe, J., Adams, S., Campillay, A., Choi, C., Contreras, C., Dietrich, M., Dubberley, M., Elphick, M., Foale, S., Giustini, M., Gonzalez, C., Hawkins, E., Howell, D.A., Hsiao, E.Y., Koss, M., Leighly, K.M., Morrell, N., Mudd, D., Mullins, D., Nugent, J.M., Parrent, J., Phillips, M.M., Pojmanski, G., Rosing, W., Ross, R., Sand, D., Terndrup, D.M., Valenti, S., Walker, Z., Yoon, Y., 2014. The Man behind the Curtain: X-Rays Drive the UV through NIR Variability in the 2013 Active Galactic Nucleus Outburst in NGC 2617. *ApJ* 788, 48. doi:[10.1088/0004-637X/788/1/48](https://doi.org/10.1088/0004-637X/788/1/48), [arXiv:1310.2241](https://arxiv.org/abs/1310.2241).
- Shibata, K., Magara, T., 2011. Solar Flares: Magnetohydrodynamic Processes. *Living Reviews in Solar Physics* 8, 6. doi:[10.12942/lrsp-2011-6](https://doi.org/10.12942/lrsp-2011-6).
- Shui, Q.C., Li, D.Y., Zhou, C., Zhao, G.Y., Zheng, T.C., Yuan, W., Einstein Probe Team, 2024. EP trigger ID 01709061302: the X-ray transient is likely a stellar flare event. *GRB Coordinates Network* 37615, 1. URL: <https://ui.adsabs.harvard.edu/abs/2024GCN.37615...1S>.
- Smith, R.K., Brickhouse, N.S., Liedahl, D.A., Raymond, J.C., 2001. Collisional Plasma Models with APEC/APED: Emission-Line Diagnostics of Hydrogen-like and Helium-like Ions. *ApJL* 556, L91–L95. doi:[10.1086/322992](https://doi.org/10.1086/322992), [arXiv:astro-ph/0106478](https://arxiv.org/abs/astro-ph/0106478).
- Steinmetz, M., Guiglion, G., McMillan, P.J., Matijević, G., Enke, H., Kordopatis, G., Zwitter, T., Valentini, M., Chiappini, C., Casagrande, L., Wojno, J., Anguiano, B., Bienaymé, O., Bijaoui, A., Binney, J., Burton, D., Cass, P., de Laverny, P., Fiegert, K., Freeman, K., Fulbright, J.P., Gibson, B.K., Gilmore, G., Grebel, E.K., Helmi, A., Kunder, A., Munari, U., Navarro, J.F., Parker, Q., Ruchti, G.R., Recio-Blanco, A., Reid, W., Seabroke, G.M., Siviero, A., Siebert, A., Stupar, M., Watson, F., Williams, M.E.K., Wyse, R.F.G., Anders, F., Antoja, T., Birko, D., Bland-Hawthorn, J., Bossini, D., García, R.A., Carrillo, I., Chaplin, W.J., Elsworth, Y., Famaey, B., Gerhard, O., Jofre, P., Just, A., Mathur, S., Miglio, A., Minchev, I., Monari, G., Mosser, B., Ritter, A., Rodrigues, T.S., Scholz, R.D., Sharma, S., Sysoliatina, K., RAVE Collaboration, 2020. The Sixth Data Release of the Radial Velocity Experiment (RAVE). II. Stellar Atmospheric Parameters, Chemical Abundances, and Distances. *AJ* 160, 83. doi:[10.3847/1538-3881/ab9ab8](https://doi.org/10.3847/1538-3881/ab9ab8), [arXiv:2002.04512](https://arxiv.org/abs/2002.04512).
- Stelzer, B., Neuhäuser, R., Casanova, S., Montmerle, T., 1999. Rotational modulation of X-ray flares on late-type stars: T Tauri stars and Algol. *A&A* 344, 154–162. doi:[10.48550/arXiv.astro-ph/9901317](https://doi.org/10.48550/arXiv.astro-ph/9901317), [arXiv:astro-ph/9901317](https://arxiv.org/abs/astro-ph/9901317).
- Tsuboi, Y., Yamazaki, K., Sugawara, Y., Kawagoe, A., Kaneto, S., Iizuka, R., Matsumura, T., Nakahira, S., Higa, M., Matsuoka, M., Sugizaki, M., Ueda, Y., Kawai, N., Morii, M., Serino, M., Mihara, T., Tomida, H., Ueno, S., Negoro, H., Daikyuji, A., Ebisawa, K., Eguchi, S., Hiroi, K., Ishikawa, M., Isobe, N., Kawasaki, K., Kimura, M., Kitayama, H., Kohama, M., Kotani, T., Nakagawa, Y.E., Nakajima, M., Ozawa, H., Shidatsu, M., Sootome, T., Sugimori, K., Suwa, F., Tsunemi, H., Usui, R., Yamamoto, T., Yamaoka, K., Yoshida, A., 2016. Large X-ray flares on stars detected with MAXI/GSC: A universal correlation between the duration of a flare and its X-ray luminosity. *PASJ* 68, 90. doi:[10.1093/pasj/psw081](https://doi.org/10.1093/pasj/psw081), [arXiv:1609.01925](https://arxiv.org/abs/1609.01925).
- Tsuru, T., Makishima, K., Ohashi, T., Inoue, H., Koyama, K., Turner, M.J.L., Barstow, M.A., McHardy, I.M., Pye, J.P., Tsunemi, H., Kitamoto, S., Taylor, A.R., Nelson, R.F., 1989. X-ray and radio observations of flares from the RS Canum Venaticorum system UX Arietis. *PASJ* 41, 679–695. URL: <https://ui.adsabs.harvard.edu/abs/1989PASJ...41..679T>.
- Veronig, A., Vršnak, B., Temmer, M., Hanslmeier, A., 2002. Relative timing of solar flares observed at different wavelengths. *Sol. Phys.* 208, 297–315. doi:[10.1023/A:1020563804164](https://doi.org/10.1023/A:1020563804164), [arXiv:astro-ph/0208088](https://arxiv.org/abs/astro-ph/0208088).
- Vida, K., Kővári, Z., Leitzinger, M., Odert, P., Oláh, K., Seli, B., Kriskovics, L., Greimel, R., Görgei, A.M., 2024. Stellar Flares, Superflares, and Coronal Mass Ejections—Entering the Big Data Era. *Universe* 10, 313. doi:[10.3390/universe10080313](https://doi.org/10.3390/universe10080313), [arXiv:2407.16446](https://arxiv.org/abs/2407.16446).
- Voges, W., Aschenbach, B., Boller, T., Braeuninger, H., Briel, U., Burkert, W., Dennerl, K., Enghauser, J., Gruber, R., Haberl, F., Hartner, G., Hasinger, G., Kuerster, M., Pfeffermann, E., Pietsch, W., Predehl, P., Rosso, C., Schmitt, J.H.M.M., Truemper, J., Zimmermann, H.U., 1999. VizieR Online Data Catalog: ROSAT All-Sky Bright Source Catalogue (1RXS) (Voges+ 1999). *VizieR On-line Data Catalog: IX/10A*. Originally published in: 1999A&A...349..389V.
- Walkowicz, L.M., Basri, G., Batalha, N., Gilliland, R.L., Jenkins, J., Borucki, W.J., Koch, D., Caldwell, D., Dupree, A.K., Latham, D.W., Meibom, S., Howell, S., Brown, T.M., Bryson, S., 2011. White-light Flares on Cool Stars in the Kepler Quarter 1 Data. *AJ* 141, 50. doi:[10.1088/0004-6256/141/2/50](https://doi.org/10.1088/0004-6256/141/2/50), [arXiv:1008.0853](https://arxiv.org/abs/1008.0853).
- Wilms, J., Allen, A., McCray, R., 2000. On the absorption of x-rays in the interstellar medium. *The Astrophysical Journal* 542, 914–924. URL: <https://doi.org/10.1086/317016>, doi:[10.1086/317016](https://doi.org/10.1086/317016).

- Wu, Y., Chen, H., Tian, H., Zhang, L., Shi, J., He, H., Lu, H., Xu, Y., Wang, H., 2022. Broadening and Redward Asymmetry of $H\alpha$ Line Profiles Observed by LAMOST during a Stellar Flare on an M-type Star. *ApJ* 928, 180. doi:[10.3847/1538-4357/ac5897](https://doi.org/10.3847/1538-4357/ac5897), [arXiv:2203.02292](https://arxiv.org/abs/2203.02292).
- Yan, Y., He, H., Li, C., Esamdin, A., Tan, B.L., Zhang, L.Y., Wang, H., 2021. Characteristic time of stellar flares on Sun-like stars. *MNRAS* 505, L79–L83. doi:[10.1093/mnras1/slab055](https://doi.org/10.1093/mnras1/slab055), [arXiv:2105.12375](https://arxiv.org/abs/2105.12375).
- Yang, Z., Zhang, L., Meng, G., Han, X.L., Misra, P., Yang, J., Pi, Q., 2023. Properties of flare events based on light curves from the TESS survey. *A&A* 669, A15. doi:[10.1051/0004-6361/202142710](https://doi.org/10.1051/0004-6361/202142710).
- Yuan, W., Dai, L., Feng, H., Jin, C., Jonker, P., Kuulkers, E., Liu, Y., Nandra, K., O'Brien, P., Piro, L., Rau, A., Rea, N., Sanders, J., Tao, L., Wang, J., Wu, X., Zhang, B., Zhang, S., Ai, S., Buchner, J., Bulbul, E., Chen, H., Chen, M., Chen, Y., Chen, Y.P., Coleiro, A., Zelati, F.C., Dai, Z., Fan, X., Fan, Z., Friedrich, S., Gao, H., Ge, C., Ge, M., Geng, J., Ghirlanda, G., Gianfagna, G., Gou, L., Guillot, S., Hou, X., Hu, J., Huang, Y., Ji, L., Jia, S., Komossa, S., Kong, A.K.H., Lan, L., Li, A., Li, A., Li, C., Li, D., Li, J., Li, Z., Ling, Z., Liu, A., Liu, J., Liu, L., Liu, Z., Luo, J., Ma, R., Maggi, P., Maitra, C., Marino, A., Ng, S.C.Y., Pan, H., Rukdee, S., Soria, R., Sun, H., Tam, P.H.T., Thakur, A.L., Tian, H., Troja, E., Wang, W., Wang, X., Wang, Y., Wei, J., Wen, S., Wu, J., Wu, T., Xiao, D., Xu, D., Xu, R., Xu, Y., Xu, Y., Yang, H., You, B., Yu, H., Yu, Y., Zhang, B., Zhang, C., Zhang, G., Zhang, L., Zhang, W., Zhang, Y., Zhou, P., Zou, Z., 2025. Science objectives of the Einstein Probe mission. *Science China Physics, Mechanics, and Astronomy* 68, 239501. doi:[10.1007/s11433-024-2600-3](https://doi.org/10.1007/s11433-024-2600-3), [arXiv:2501.07362](https://arxiv.org/abs/2501.07362).
- Yuan, W., Zhang, C., Chen, Y., Ling, Z., 2022. The Einstein Probe Mission, in: Bambi, C., Sanganello, A. (Eds.), *Handbook of X-ray and Gamma-ray Astrophysics*, p. 86. doi:[10.1007/978-981-16-4544-0_151-1](https://doi.org/10.1007/978-981-16-4544-0_151-1).
- Zheng, W., Brink, T.G., Filippenko, A.V., Skemer, A., Leonhardes-Barboza, N., Forman, J., Gutierrez, M., Jones, I., Kaur, R., Mengistu, P., Patel, A., Uppal, A., Wolff, N., Woodland, M., KAIT GRB team, 2025. EP trigger ID 01709061302: Lick/Kast spectroscopy with the 3 m Shane telescope. GRB Coordinates Network 39707, 1. URL: <https://gcn.nasa.gov/circulars/39707>.